Applied Catalysis A, General 655 (2023) 119100

Contents lists available at ScienceDirect

Applied Catalysis A, General

journal homepage: www.elsevier.com/locate/apcata

PdZn/ZrO_2+SAPO-34 bifunctional catalyst for CO_2 conversion: Further insights by spectroscopic characterization

Pierfrancesco Ticali [a], Sara Morandi [a,*], Genrikh Shterk [b], Samy Ould-Chikh [b], Adrian Ramirez [b,c], Jorge Gascon [b], Sang-Ho Chung [b], Javier Ruiz-Martinez [b], Silvia Bordiga [a]

[a] Department of Chemistry, NIS Center and INSTM Reference Center, University of Turin, 10125 Turin, Italy
[b] KAUST Catalysis Center (KCC), King Abdullah University of Science and Technology, Thuwal 23955, Saudi Arabia
[c] SwissCAT+ East, ETH Zurich, Zurich 8093, Switzerland

ARTICLE INFO

Keywords:
CO_2 hydrogenation
PdZn alloy
SAPO-34
FT-IR spectroscopy of CO adsorption
NAP-XPS
Solid-state NMR

ABSTRACT

The present work aims at further investigating a previously studied PdZn/ZrO_2+SAPO-34 bifunctional catalyst for CO_2 conversion. High activity and selectivity for propane was proved and the results obtained by NAP-XPS measurements and CO adsorption at liquid-nitrogen temperature (LNT) followed by FT-IR spectroscopy are shown. After reduction, we confirmed the formation of PdZn alloy. At LNT, Pd carbonyl IR band shows a peculiar behavior linked to an intimate interaction between PdZn particles, ZnO and ZrO_2. The combined system was characterized as fresh, used and regenerated. On the fresh PdZn/ZrO_2+SAPO-34 the characteristic features of the two components do not appear perturbed by the mixing. As for the used system, the absence of Pd carbonyls and the decrease of CO on SAPO-34 Brønsted acid sites are correlated to organic species revealed by ssNMR. Regeneration in oxygen restores catalytic sites, although new Pd^{2+}/Zn^{2+} carbonyls appear due to ion exchange into SAPO-34 framework.

1. Introduction

Climate change is the most difficult challenge that humanity is trying to combat. The incessantly increase of carbon dioxide concentration reaches a new record year by year since the industrial revolution and the average of CO_2 concentration reached 418 ppm in January 2022 [1]. To date, limiting the increase of global temperature to 1.5 °C, as established by the Paris Agreement, is the real challenge. Hence, Carbon Capture Utilization and Storage (CCUS) represents the only way to reduce the CO_2 concentration and to contain the greenhouse effect.

To achieve an efficient way for the capture, conversion, transportation, and storage is economically challenging. Indeed, CCUS is not technologically ready to be applied on a global scale, demonstrating how difficult it is to find an economic way to solve global environmental issues.

One option is represented by the chemical reduction of CO_2 to obtain C_1 products [2], like methanol, and to convert methanol into hydrocarbons.

According to several works [3,4], metal/oxide systems are a good choice to perform CO_2 adsorption and conversion into methanol. Usually investigated metals [5,6] are Zn, Pt, Cu [7] and Pd [8], whereas, among supports, several oxides such as SiO_2, ZnO and ZrO_2 are used [9]. In particular, zinc plays a key role for both intermediate stabilization and H_2 heterolytic splitting thanks to its activity in inducing defects (such as oxygen vacancies) [10–13]. ZrO_2 is weakly hydrophilic and avoids water-poisoning [2,5] and it is largely reported as an excellent metal support. Indeed, this oxide shows unique surface properties: Brønsted basic sites, Lewis acidic-basic $Zr^{4+}O^{2-}$ pairs and redox activity [14,15]. All these properties are largely discussed in Li et al. [2], which exhaustively describes how ZrO_2 can be a promising candidate for CO_2-to-methanol reaction.

According to some articles[16–22], Pd-based catalysts are active for CO_2 hydrogenation to methanol with high CO_2 conversion, methanol selectivity, yield, turnover frequency and stability with a minimal composition of Pd ($\leq$ 5 wt%) and, by alloying with zinc, it seems to play a key role in hydrogen splitting, and it leads to a good conversion of CO_2 into methanol.

However, metal or oxidic phases are not capable of converting methanol into hydrocarbons. Hence, different authors [23,24] proposed bifunctional catalysts, which are made up of an oxidic phase on a zeolitic

* Corresponding author.
E-mail address: sara.morandi@unito.it (S. Morandi).

https://doi.org/10.1016/j.apcata.2023.119100
Received 15 November 2022; Received in revised form 10 February 2023; Accepted 11 February 2023
Available online 13 February 2023

support. The acid sites of zeolite are capable of binding and hydrogenating methanol molecules to produce hydrocarbons with different yield and different number of carbon atoms according to the type of the zeolite involved in the reaction [25,26]. Defining a possible route involved for the generation of different hydrocarbons is not straightforward. Over the years, three main pathways have been proposed. Chronologically, the first theorized mechanism was the one proposed by Dessau and LaPierre [27], founded on consecutive methylation and cracking, to produce ethylene and other higher alkenes over ZSM-5. The second mechanism was theorized by Dahl and Kolboe [28], based on the low reactivity of propene and ethylene when co-reacting with methanol over SAPO-34. This mechanism is based on a hydrocarbon-pool concept [29]. The most recent mechanism is represented by the dual-cycle concept, which is founded on the interconnection between an olefinic and an aromatic cycle.

To date, one of the most demanding hydrocarbons is propane. By 2025, propane will represent one of the most used hydrocarbons for industrial purposes, with a market growth of 5% per year [30].

We have recently published interesting results about PdZn/ZrO_2 catalyst in combination with SAPO-34 exploited in the CO_2 adsorption and conversion with propane as the main product [31]. According to our previous work and to the best of our knowledge, this system shows very good propane yields, which have never been reported about CO_2 valorization with a meaningful C_{2+} hydrocarbon conversion [32]. In particular, we demonstrated by XAS and FT-IR spectroscopy that a PdZn alloy is formed during catalyst activation. The alloy is in intimate contact with oxygen-vacancy rich ZnO particles over the ZrO_2 support and, when it is exposed to the CO_2-containing reaction feed, develops into a core-shell structure with a PdZn alloy surrounded by a polycrystalline ZnO shell. PdZn alloy is directly responsible for the MeOH formation on the PdZn/ZrO_2 component. MeOH reacts over the SAPO-34 following a classical MTO mechanism with propane as the main product [31]. The intimate mixture of both PdZn/ZrO_2 and SAPO-34 causes an instant MeOH consumption, increasing the CO_2 conversion and reducing drastically the CO selectivity. In the previous work, the characterization of the PdZn/ZrO_2 phase was reported, but the paper lacks the spectroscopic characterization of the PdZn/ZrO_2+SAPO-34 combined system.

Hence, in this work, we are going to present some new catalytic results, which are in line with those already presented in our former work, in any case. In order to achieve a more comprehensive understanding of the bifunctional system, using CO as probe molecule, we are going to focus on the spectroscopic characterization of the combined system, taking the moves from a more detailed FT-IR characterization of the PdZn/ZrO_2 component, which was also further investigated by near ambient pressure X-ray photoelectron spectroscopy. By means of solid-state nuclear magnetic resonance, we proposed an elucidation of the organic species trapped inside the SAPO-34 during catalytic runs.

2. Experimental section

2.1. Catalyst preparation

Catalyst preparation steps are described in details in our former paper [31]. Summarizing in brief, the PdZn/ZrO_2 catalyst was prepared by a colloidal impregnation method starting from palladium and zinc acetate solutions in DMF and ethylene glycol, respectively. The obtained colloidal mixture, after washing and dispersion in ethanol, was added with zirconium hydroxide, $Zr(OH)_4$, in order to obtain a molar composition of 2% Pd, 13% Zn and 85% Zr, verified by Energy-dispersive X-ray spectroscopy (EDS). The final catalyst was obtained after drying and calcination at 500 °C. As for SAPO-34, it was purchased from ACS materials (SiO_2/Al_2O_3 =0.5).

The combined system was produced by mixing the oxidic phase with the zeotype by mortar and pestle in a 1:1 wt ratio.

2.2. Catalytic tests

Catalytic tests were executed in a 4 channel Flowrence® from Avantium. 50 mg of the stand-alone PdZn/ZrO_2 catalyst or 100 mg of the combined PdZn/ZrO_2+SAPO-34 catalyst were typically used. The gas feed composition was: 24 vol% of CO_2, 72 vol% of H_2 and 4 vol% of He as internal standard. Before feeding the reaction mixture, all samples were reduced in situ with a pure H_2 atmosphere for 4 h at 400 °C. The tubes were then pressurized to 30 bar using a membrane-based pressure controller.

GC is an Agilent 7890B with two sample loops. One sample loop goes to TCD channel with 2 Haysep pre-column and MS5A, where He, H_2, CH_4 and CO are separated. Another sample loop goes to a FID with an Innowax pre-column, a Gaspro column and another Innowax column. Gaspro column separates C_1-C_8, paraffins and olefins, while Innowax column separates oxygenated and aromatics.

Conversion and selectivity are reported on C_1 basis and are defined as follows:

$$Conv_{CO_2}(\%) = \frac{CO_{2blk}/He_{blk} - CO_{2R}/He_R}{CO_{2blk}/He_{blk}} \times 100$$

$$S_{Cn}(\%) = \frac{n \cdot \frac{C_{Cn,R}}{C_{He,R}}}{\left(\frac{C_{CO_2,blk}}{C_{He,blk}} - \frac{C_{CO_2,R}}{C_{He,R}}\right)} \bullet 100$$

where $C_{i,blk}$ and $C_{i,R}$ are the concentrations determined by GC analysis in the blank and in the reactor outlet, respectively. Carbon balance closure was better than 2.5% in all cases.

For the ^{13}C labeled tests aimed at ssNMR measurements (vide infra) the same Flowrence® set up was used. The labeled $^{13}CO_2/H_2$ mixture (100 bar lecture bottle) was provided by CK Isotopes Limited.

2.3. Spectroscopic characterization

Absorption IR spectra were collected using a Perkin-Elmer FTIR 2000 spectrophotometer equipped with a Hg-Cd-Te cryo-detector, at a resolution of 2 cm^{-1} in the range of wavenumbers 7200–580 cm^{-1}. All sample powders were compressed in self-supporting discs (~20 mg cm^{-2}) and placed in a quartz IR cell suitable for thermal treatments in controlled atmosphere and spectra recording at room and liquid-nitrogen temperature (RT and LNT, respectively).

Before IR measurements, all the samples were outgassed at 400 °C for 30 mins and then reduced with 40 mbar of dry hydrogen at 400 °C for 30 mins. The reduction treatment aims at simulating the reduction step performed before the catalytic tests. From now on, we will name all the pre-reduced catalysts as “activated” catalysts.

After activation, FT-IR spectra were run at increasing CO pressure up to 20 mbar at RT and LNT on PdZn/ZrO_2 catalyst and at LNT on SAPO-34 and PdZn/ZrO_2+SAPO-34 combined system. CO was used as probe molecule in order to characterize surface sites, such as Pd sites, Lewis acid sites ($Zr^{4+}$and Zn^{2+}) and Brønsted acid sites of SAPO-34. Moreover, CO adsorption was performed on PdZn/ZrO_2+SAPO-34 combined system after catalytic tests performed at 350 °C for 48 h, at 30 bar, with space velocity of 12000 ml g^{-1} h^{-1}. The used bifunctional system was characterized before and after a regeneration step. The used catalyst was activated as already mentioned for the fresh one, while the regeneration step was performed via oxidation in dry oxygen at 600 °C (for 30 mins) and then activation in hydrogen at 400 °C (for 30 mins), in order to simulate the regeneration conditions carried out before the catalytic tests reported in the previous work [31].

Near Ambient Pressure (NAP)-XPS measurements were carried out using an EnviroESCA spectrometer (SPECS GmbH) equipped with a monochromatic Al Kα X-ray source (hν = 1486.71 eV) operating at 42 W and X-ray emission of 3.00 mA. Typically, the PdZn/ZrO_2 catalyst was mixed with carbon black powder in ratio 10:1 to avoid an excessive

charging of the surface and then pressed into a pellet (d=2 mm, h=0.5 mm) within the central cavity of a steel plate. Resistive heating was carried out by a button heater (SPECS GmbH). Temperature set-points for degassing and reduction of 400 °C were reached through manual ramping over a period of 30 min. High resolution spectra were obtained at energy pass of 10 eV; dwell time of 0.5 s per point and step of 0.1 eV were used for all regions (Zr(3d), C(1s), Pd(3d), O(1s) and Zr (2p)).

$PdZn/ZrO_2$ sample was measured with HR-XPS before NAP experiments. The sample was outgassed in the loading chamber for 1 h at 400 °C under UHV conditions. Subsequently, to obtain the activated sample, a flow of 40 ml/min of H_2 at 20 mbar was applied for 2 h. After reduction, the sample was transferred to the analysis chamber for further HR-XPS measurement.

All ^1H and ^{13}C related (both 1D and 2D) MAS ssNMR spectroscopic experiments were performed on Bruker AVANCE III spectrometers operating at 600 MHz frequency for ^1H using a conventional double resonance 3.2 mm MAS HXY probe. ^1H and ^{13}C NMR chemical shifts are reported with respect to the external reference adamantane. All NMR measurements were performed at room temperature and MAS frequency of 20 kHz. Herein, samples were prepared using fully enriched $^{13}CO_2$ at experimental conditions (30 bar, 375 °C, H_2:$^{13}CO_2$ = 3, and 10000 ml g^{-1} h^{-1}, 60 h) suitable to increase the ssNMR sensitivity. A dual-bed configuration was used, instead of a mechanical mixture of the standard catalytic tests, in order to be able to perform measurements on used SAPO-34 alone. The 1D direct excitation (DE) 1 H-13 C cross-polarization (CP) spectra were recorded using a 4 s recycle delay. The 1D insensitive nuclei enhanced by polarization transfer (INEPT) spectrum was recorded using a 2 s recycle delay, a 20 ms acquisition time and accumulation of 4 k scans. 1 H and 13 C pulses were applied with a field strength of 70 and 50 kHz, respectively. 2D ^{13}C–^{13}C spectra were recorded using a 2 s recycle delay, 10 ms (F2) and 1.3 ms (F1) acquisition time and an accumulation of 256 scans. ^{13}C–^{13}C mixing was achieved through proton driven spin-diffusion (PDSD) using phase-alternated-recoupling-irradiation-schemes (PARIS) for 120 ms (CP). 70 kHz SPINAL64 ^1H decoupling was applied during both direct and indirect dimensions. To probe mobile molecules, 2D ^1H–^{13}C INEPT-based heteronuclear correlation (HETCOR) was applied with 1.5 s recycle delay, 17 ms (13 C, F2) and 4 ms (1 H, F1) acquisition time and an accumulation of 512 scans. To probe rigid molecules, dipolar based ^1H–^{13}C-^1H HETCOR correlation spectra were obtained using a fixed 0.5 ms contact time for both ^1H–^{13}C CP and ^{13}C–^1H CP periods. Background signals were suppressed by an 8 kHz MISSISSIPPI block ($\tau = 5$ ms, $N = 2$) before the last CP period. ^{13}C PISSARRO (phase inverted supercycled sequence for attenuation of rotary resonance) decoupling was applied during acquisition. The recycle delay was 2 s, acquisition times 10 ms (F2, ^1H) and 2 ms (F1, ^{13}C) and number of scans 64. All NMR spectra were processed and analyzed using Bruker TopSpin version 3.6.3.

3. Results and discusion

3.1. Catalytic performance of the $PdZn/ZrO_2$ and $PdZn/ZrO_2$+SAPO-34 catalysts

In our previous work [31], we reported a catalytic screening over the stand-alone $PdZn/ZrO_2$ catalyst and its combination with SAPO-34, focusing these control experiments on monitoring MeOH selectivity for $PdZn/ZrO_2$ and that of propane for the bifunctional system at different reaction pressures and temperatures. Moreover, for the bifunctional system, detailed hydrocarbon distribution for the CO_2 conversion was reported as a function of space velocity. Here we focus on CO, MeOH and CH_4 selectivity for $PdZn/ZrO_2$ at constant pressure and different temperatures and space velocities and on the detailed hydrocarbon distribution as a function of time for the bifunctional system.

An overview of the catalytic performance of the stand-alone $PdZn/ZrO_2$ catalyst at different reaction conditions is shown in Table 1. We can observe that CO_2 conversion and MeOH/CO selectivity are in clear agreement with the process thermodynamics [32]. In particular, increasing the temperature or decreasing the gas hourly space velocity (GHSV) increases the CO_2 conversion. On the other hand, this conversion increase is accompanied by a MeOH selectivity decrease and the subsequent CO selectivity increase. The highest methanol selectivity was therefore obtained at the lowest temperature and highest GHSV (74.1%, 250 °C and 12000 ml g^{-1} h^{-1}). Looking at the methanol yield, the best condition was found at 250 °C, 30 bar and 3000 ml g^{-1} h^{-1} (5.1% yield). Lastly, methane selectivity is negligible (below 0.1–0.5%) at all tested conditions.

An overview of the catalytic performance of the combined $PdZn/ZrO_2$+SAPO-34 system is shown in Fig. 1. We can observe that the addition of SAPO-34 successfully converts the MeOH produced on the first $PdZn/ZrO_2$ component into a series of hydrocarbons, with the C_3 family dominating the distribution, in line with the expected behavior of the system [31]. CO_2 conversion and CO selectivity remain in similar levels of the stand-alone $PdZn/ZrO_2$. With the evolution of the reaction with time, we can observe that deactivation starts to occur and, at around 38 h on stream, DME starts being produced. This DME formation is a clear sign of the SAPO-34 component deactivation and it fully dominates the hydrocarbon distribution after 50 h on stream.

3.2. CO adsorption on $PdZn/ZrO_2$ catalyst

Fig. 2-a reports FT-IR spectra of CO adsorbed at RT and at increasing pressure on the activated $PdZn/ZrO_2$ catalyst: an asymmetric band in the region between 2080 and 2020 cm^{-1} appears and increases in intensity upon CO pressure increase. For sake of clarity, we opted to show the FT-IR spectra related to CO adsorption at RT, despite they have been already displayed in our previous work [31], in order to compare them with those obtained at LNT.

As described in our previous work [31], the band is ascribed to Pd^0 linear carbonyls [33]. However, the frequency of the maximum, quite lower with respect to that characteristic of linear carbonyls on reduced Pd supported particles, and the absence of bridged CO species in the region 2000–1970 cm^{-1} prove the presence of PdZn alloy [34–36]. Since Zn is markedly more abundant than Pd, PdZn particles are in intimate contact with ZnO particles over the ZrO_2 support, as well evidenced by high-resolution HAADF-STEM images in our previous work [31]. More in details, the linear carbonyl band is constituted by several components (see inset of Fig. 2-a): the most intense one lies at 2063 cm^{-1} and shifts to 2069 cm^{-1} at the maximum CO coverage (θ_{CO}, from blue to red line), whereas two shoulders are evident at 2071 cm^{-1} (2074 cm^{-1} for the maximum θ_{CO}, red line) and 2048 cm^{-1}.

As just mentioned in our former work [31], Pd^0-CO bond shows

Table 1
Overview of the catalytic performance of the stand-alone $PdZn/ZrO_2$ catalyst at different reaction conditions. H_2/CO_2 ratio of 3, 30 bar and 24 h T.O.S.

Temp (°C)	GHSV (ml g^{-1} h^{-1})	Conversion (%)	Sel CO (%)	Sel MeOH (%)	Sel CH_4 (%)	MeOH Yield (%)
250	12000	3.8	25.7	74.1	0.2	2.8
300		9.2	68.3	31.6	0.1	2.9
350		20.8	83.2	16.7	0.1	3.5
400		28.2	96.5	3.4	0.2	1.0
250	6000	6.9	34.6	65.3	0.1	4.5
300		14.1	76.7	23.2	0.0	3.3
350		21.7	89.2	10.8	0.1	2.3
400		28.2	96.8	3.1	0.2	0.9
250	3000	9.0	42.8	57.1	0.1	5.1
300		15.4	82.1	17.8	0.1	2.7
350		21.7	90.8	9.2	0.2	2.0
400		28.2	96.8	3.0	0.5	0.8

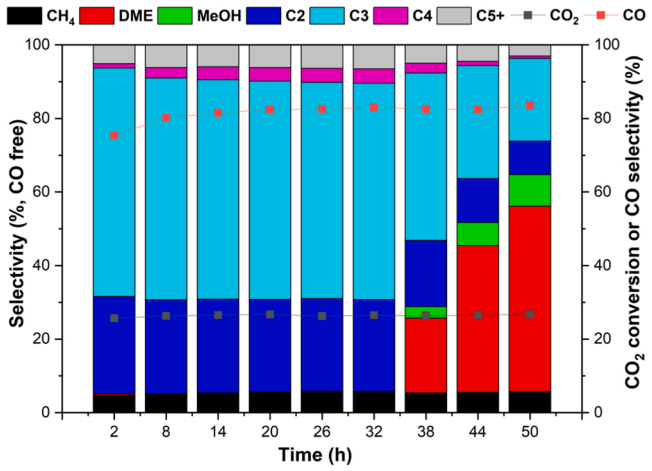

Fig. 1. Overview of the catalytic performance of the combined PdZn/ZrO_2+SAPO-34 system. H_2/CO_2 ratio of 3, 350 °C and 12000 ml g^{-1} h^{-1}.

strong π-backdonation character, thus the lower the band frequency the more coordinatively unsaturated the site [37]. That being said, we assign the shoulder at 2048 cm^{-1} to carbonyls of highly defective Pd^0 sites, e.g. corners, the main component at 2063–2069 cm^{-1} to carbonyls of less defective sites, e.g. edges, whereas the shoulder at 2071–2074 cm^{-1} can be related to terrace sites.

The blue-shift of the main peak and shoulders is explained taking into account the dipolar coupling and the "*chemical effect*" [38]. The first one can be neglected in our case due to the presence of Pd dilution by alloying with Zn, which lowers the dipole-dipole interaction between neighboring CO molecules adsorbed on Pd. The second one is related with the decrease of π-backdonation as the number of adsorbed CO molecules increases, so that the CO bond strength and, consequently, the stretching frequency increases upon increasing θ_{CO}.

After outgassing (dashed black line in Fig. 2-a), the intensities of the main peak and shoulders are drastically reduced but not totally brought down, evidencing a certain stability of Pd^0-CO at room temperature. The outgassing decreases the effect due to the θ_{CO}, i.e. the "*chemical effect*", shifting back the absorptions to their former positions.

In order to characterize Lewis acid sites (i.e. Zr^{4+} and Zn^{2+}) and eventually Zn^0, CO adsorption was performed at liquid-nitrogen temperature on the activated PdZn/ZrO_2 catalyst (Fig. 2-b). Two bands are present: the former in the range 2080–2020 cm^{-1} is related to CO linearly adsorbed on metallic palladium sites in the PdZn alloy, the latter in the range 2190–2120 cm^{-1} is related to CO adsorption on Zr^{4+} and Zn^{2+} sites.

As for the high-frequency region, the first appearing band at 2180 cm^{-1} (Fig. 2-b, green line) could be related to zinc(II)-carbonyls [33,39]: this very weak band is completely covered by the Zr^{4+}-CO band at higher CO doses. Zr^{4+}-CO band exhibits a red-shift up to 2155 cm^{-1} due to the "*chemical effect*": Zr^{4+} is a σ-donor center, hence the frequency of the peak red-shifts as the CO coverage increases [33, 40]. These findings are in line with those reported by Ticali et al. [41] for $ZnZrO_X$ systems: among the three samples analyzed, the one with the highest concentration of Zn was featured by the formation of a ZnO extra-phase that could be looked at as a Zn/ZrO_2 system. As reported, the authors highlighted that the same spectroscopic features could be mainly assigned to Zr^{4+} with different coordination, while Zn^{2+} could only give a minor contribution to the band.

As for Zn^0 sites, to the best of our knowledge no literature data are available about the Zn^0-CO species, reasonably because d-orbitals of Zn^0 are not suitable to form stable carbonyl species. For this reason, some authors used bands related to Zn^{2+} carbonyls on oxidized and reduced supported zinc to evaluate, by subtraction, the amount of Zn^0 formed in reduction processes [42]. These literature data highlight that Zn^0 carbonyls are not observable species.

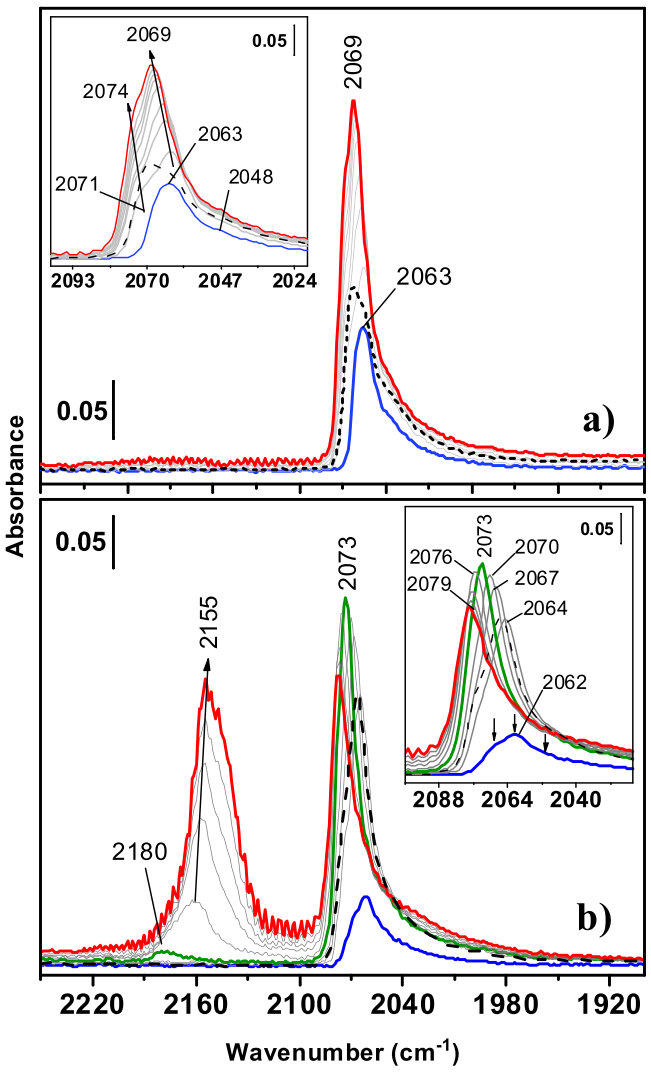

Fig. 2. a) FT-IR spectra of CO adsorbed at RT on activated PdZn/ZrO_2 catalyst. Spectra were acquired at increasing CO pressure up to 20 mbar (from blue to red line) and after outgassing (dashed black line). b) FT-IR spectra of CO adsorbed at LNT on activated PdZn/ZrO_2 catalyst. Spectra were acquired at increasing CO pressure up to 20 mbar (from blue to red line) and after outgassing (dashed black line). The green line represents the CO pressure ("*breakdown*" pressure) beyond which Zn^{2+}-CO and Zr^{4+}-CO bands pop up and Pd^0-CO band starts decreasing.

Focusing on the Pd^0 region, as observed at RT, the carbonyl band show at least three components (evidenced by arrows in the inset of Fig. 2-b), which put in evidence the different Pd sites in the alloy, as just discussed for Fig. 2-a. Differently from CO adsorption at RT, it is worth to note a peculiar behavior when CO is adsorbed at increasing doses: from the blue line, through the green line, to the red line, the spectra highlight an increasing and then a decreasing intensity of Pd carbonyl band along with a continuous shift to higher frequencies. From now on we will call this behavior "*bell-shaped shift*". This shift is featured by a maximum reached by the Pd carbonyl band (green line) at a pressure that we call "*breakdown*" pressure. After the "*breakdown*" pressure, as CO coverage increases, the band of CO on cationic sites in the region 2190–2120 cm^{-1} suddenly increases becoming well evident, but the absorption of CO on Pd^0 atoms decreases in intensity.

After outgassing (dashed line in Fig. 2-b), Pd^0-CO band goes back to the position and intensity of the spectrum collected after the second CO admission, just like their analogous in Fig. 2-a. The intensity of the Pd^0-

CO band after outgassing is nearly the same reached for the maximum CO pressure (red line), while CO molecules on Zr^{4+} and Zn^{2+} are completely desorbed.

The comprehension of the intensity modulation that causes the "*bell-shaped shift*" is not straightforward. The blue-shift of the Pd^0-CO band upon increasing CO pressure is similar to that observed at RT. The different behavior of this band at LNT is related to the loss of intensity that starts when CO is adsorbed on ZnO and zirconia support. This loss could be related to a diminution of the amount of CO molecules adsorbed on Pd; however, due to the lowering of the "*chemical effect*" upon decreasing CO coverage, this should cause a red-shift of the band. Alternatively, the intensity loss could be explained by a decrease of the absorption coefficient of Pd carbonyls, possibly induced by CO adsorption on ZnO and zirconia support; as a consequence, the absorption intensity decreases even if the amount of CO molecules on Pd increases. This last hypothesis is coherent with the behavior observed after the outgassing: by removing CO from Zr^{4+} and Zn^{2+} sites, the absorption coefficient increases again and the partial desorption of CO also from Pd causes the band red-shift. This hypothesis could be corroborated by the model describing the dipolar coupling obtained by Hammaker, Francis and Eischens (HFE) in 1965 [43] and subsequently modified [37,44]. As a matter of fact, the modified HFE model predicts that the dipolar coupling causes two effects observable upon increasing interacting adsorbed molecules: a shift of the absorption band at higher frequency and a reduction of the absorption coefficient. The dipolar coupling and, thus, these effects occur when adsorbed molecules belong to the same surface species, i.e. adsorbed molecules with the same singleton frequency. As a consequence, CO molecules adsorbed on ZnO and zirconia support cannot directly be responsible for the observed behavior. Moreover, due to the presence of the alloy, the dipolar coupling for CO adsorbed on Pd was previously excluded. However, the adsorption at LNT leads, reasonably, to the adsorption of a much higher amount of CO on Pd with respect to RT, which is hidden by the intensity loss. This could make the dipolar coupling to occur also for Pd in the alloy, and this is proved by the frequency at maximum coverage that is 10 cm^{-1} higher at LNT (2079 cm^{-1}) than at RT (2069 cm^{-1}). In addition, an effect of the presence of CO adsorbed on ZnO and zirconia support on the molecule proximity in the Pd carbonyl adlayer cannot be ruled out. This last should imply a strong interaction between PdZn alloy particles and the oxidic phases. Actually, HAADF-STEM images reported in our previous work [31] showed PdZn particles in intimate contact with ZnO over the ZrO_2 support.

3.3. *Near ambient pressure X-ray photoelectron spectroscopy on PdZn/ZrO_2*

In an attempt to determine the different Pd and Zn chemical species on the surface of the activated PdZn/ZrO_2 catalyst, a set of NAP-XPS experiments was performed (see Fig. 3).

The formation of PdZn alloys has been previously studied using model systems [45–48]. These studies demonstrated a shift in the $Pd^0(3d_{5/2})$ peak towards higher binding energies (from 335 to 336.1 eV) as a result of alloy formation [45,49]. The nature of such energy shifts in PdZn alloys and the effect of the alloying upon CO adsorption was studied by Rodriguez [50]. A combination of MO-SCF calculations and XPS showed that Pd(4d)→Zn(4p) charge transfer and Pd(4d)→Pd(5 s, 5p) rehybridization during alloy formation are responsible for the binding energy shift and for a weakening of Pd(4d)→CO(2π) bonding interactions [50]. More recent studies on Pd-Zn interaction reported that the charge transfer induces a negative charge over Pd and a positive charge over Zn, which should imply a reverse shift with respect to that observed [46,51,52]. However, the shift of Pd(3d) and Zn(2p) bands to

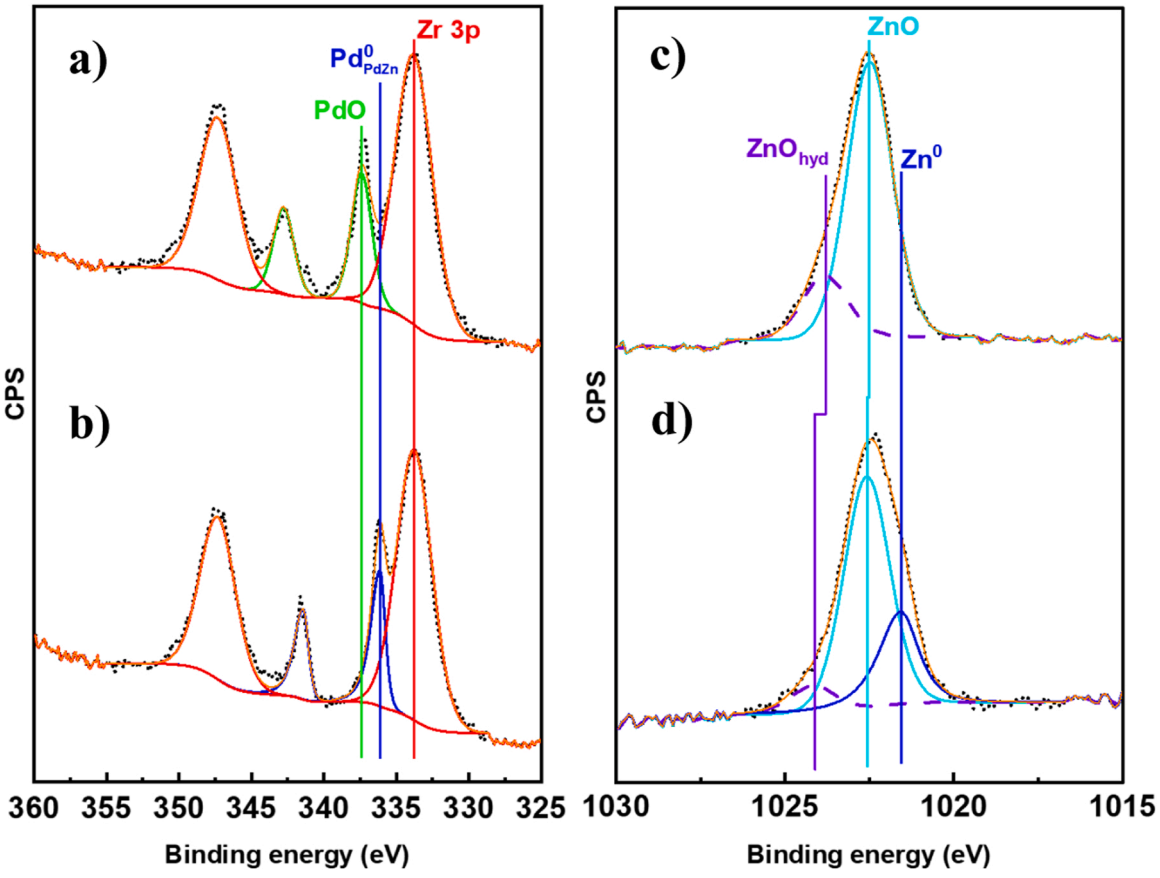

Fig. 3. NAP-XPS spectra of Pd(3d) and Zn($2p_{3/2}$) regions of PdZn/ZrO_2 catalyst as prepared (a, c) and after activation in H_2 (b, d).

higher and lower binding energies, respectively, are largely accepted as fingerprints for PdZn alloying also in more recent literature [46,47,53,54]. In the pristine PdZn/ZrO_2 catalyst (Fig. 3(a,c)), the presence of native PdO (Pd $3d_{5/2}$ 337.4 eV) and ZnO (Zn $2p_{3/2}$ 1022.5(6) eV) [55] with an atomic ratio Pd/Zn of 1.1 (Table S1), in good agreement with previous paper [31], is observed. The calculated binding energies for the Pd(3d) region are slightly higher (0.4–0.2 eV) than previously reported in literature [55–57] for Pd^{2+}.

This is probably due to charging of the sample surface and uncertainty of fitting due to overlapping with Zr(3p). The feature at ~1024 eV present in the Zn($2p_{3/2}$) region can either be attributed to Zn attached to hydroxyl groups of the ZrO_2 surface [58] or to a differential charging effect that would result in an asymmetry of the ZnO peak.

After activation at 400 °C under 20 mbar of hydrogen (Fig. 3(b, d)), full and partial reduction of Pd and Zn, respectively, are observed, with binding energies of 336.1 eV and 1021.5 eV. In contrast, when a reference sample based on Pd foil was submitted to similar conditions (Fig. S1), analysis of the XPS spectrum of the sample revealed a Pd($3d_{5/2}$) binding energy of 335.1 eV, 1 eV lower than that observed for the PdZn/ZrO_2 catalyst after reduction. These results demonstrate the formation of the aforementioned alloy and are in good agreement with the literature [36,45,46,48,49,58]. The partial reduction of Zn is in good agreement with the results reported in our previous paper, in which XAS measurements demonstrated the presence of a defective ZnO phase after reduction [31]. In addition, the Pd/Zn atomic ratio remains almost unchanged upon reduction (Table S1).

3.4. CO adsorption on SAPO-34 and PdZn/ZrO_2+SAPO-34 combined system

In order to characterize the combined bifunctional system, FT-IR measurements of CO adsorption at LNT on both fresh and used PdZn/ZrO_2+SAPO-34 system were performed after activation and reported in Fig. 4 (sections b and c, respectively). For comparison purposes, the same measurement was performed on SAPO-34 alone (section a). In all the spectra, two main peaks at 2170 and 2140 cm^{-1} are evident. The former is related to CO adsorbed on Brønsted acid sites of the zeotype material, and it grows first. The latter is assigned to liquid-like CO entrapped inside the pores of SAPO-34 [59]. When a high fraction of Brønsted acid sites is engaged in interaction with CO, the band representing liquid like CO entrapped inside the cavities starts to increase. Another band at about 2090 cm^{-1}, which was observed in some works [60,61] for Ca-Y and Na-ZSM-5, is present. This band changes frequency according to the nature of coordinated metal or cation. Indeed, the

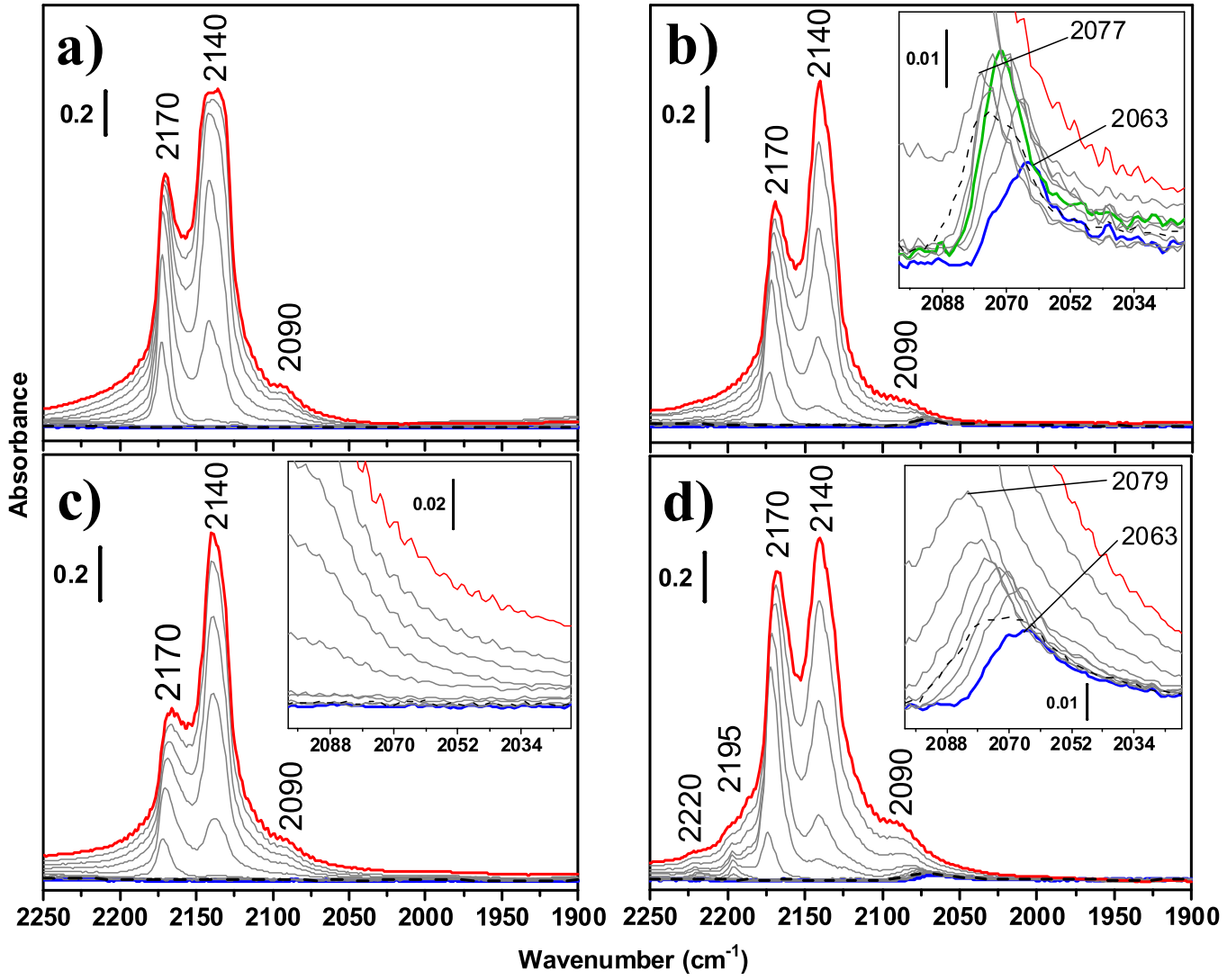

Fig. 4. FT-IR spectra of CO adsorbed at LNT on the following activated systems: SAPO-34 (a), fresh PdZn/ZrO_2+SAPO-34 (b), used PdZn/ZrO_2+SAPO-34 (c) and used PdZn/ZrO_2+SAPO-34 after regeneration in O_2 at 600 °C and activation step (d). Spectra were acquired at increasing CO pressure up to 20 mbar (from blue to red line) and after outgassing (dashed black line). Green line in section b): CO "*breakdown*" pressure for Pd carbonyls.

σ-coordinated CO through the C-end could interact with the lattice via the O-end with a guest cation (e.g. Ca [60] and Na [61] ions) or any other Lewis acid site on the surface. Another hypothesis assign this band to CO in interaction with framework oxygen atoms [62].

When SAPO-34 is mixed with PdZn/ZrO_2, nothing seems to change for the previously mentioned peaks, except a slight change in their relative intensities. Moreover, Fig. 4-b shows that the spectra of the fresh physical mixture still present the characteristic "*bell-shaped shift*" pattern in the region related to Pd^0 carbonyls (see zoom in the inset). However, Pd^0-CO pattern is no more evident on the used system (Fig. 4-c), reasonably due to the presence of coke and some other products obtained during the catalytic tests. In order to verify the possibility of having PdZn/ZrO_2 surface covered by reaction products, we performed UV-Raman characterization, which was reported in our previous manuscript [31]. UV-Raman results obtained for the combined system showed the presence of alkenes and polycyclic aromatic hydrocarbons, which is a typical feature for an initial deactivation of the catalyst. Indeed, the presence of hydrocarbon residues decreases the amount of Brønsted acid sites of SAPO-34 as evidenced by the lower intensity of the band at 2170 cm^{-1} with respect to that observed for the fresh combined system (compare Fig. 4-c and b).

In the light of the just mentioned findings, we performed a regeneration of the used combined system at 600 °C in O_2, in order to "clean" the surface from hydrocarbon residues, and then a reduction in H_2 at 400 °C to obtain the activated system. Fig. 4-d displays that Pd is available again for CO adsorption, as evidenced by the "*bell-shaped shift*" pattern in the inset, and that Brønsted acid sites of SAPO-34 are restored, as evidenced by the increased intensity of the band at 2170 cm^{-1}. Hence, we can assure that regeneration is mandatory to restore the catalytic activity of the combined system. Indeed, the catalytic tests on the regenerated sample reported in our previous paper showed a complete regained activity [31]. However, after having regenerated (i.e. oxidized) and reduced the sample, spectra are not the same as those in Fig. 4-b for the fresh combined system. Indeed, at first look the intensity ratio of the main two peaks at 2170 and 2140 cm^{-1} is changed, and they look almost equally high. Moreover, two more peaks are visible at 2220 and 2195 cm^{-1}, which can be assigned to some metallic ions exchanged with SAPO-34 Brønsted acid sites, i.e. Zn^{2+} or Pd^{2+} carbonyls [33,63]. In case of Pd carbonyls, both peaks can be attributed to dicarbonyls of isolated Pd^{2+} [33,64,65], whereas for Zn^{2+} only one band related to mono-carbonyls is reported in literature [33,63]. It is reasonable that this exchange occurs during the regeneration treatment in oxygen and that these isolated Zn^{2+}/Pd^{2+} cations are stabilized by the zeotype framework, which prevents their reduction during the subsequent treatment in hydrogen. The choice of using a regeneration temperature (600 °C) above the calcination one (500 °C) was made to completely remove coke from SAPO-34 surface.

3.5. Elucidation of molecular structure of organic species trapped in SAPO-34

To elucidate the molecular structure of zeotype-trapped organic species, we performed solid-state NMR spectroscopy (ssNMR) on the post-reacted zeotype (SAPO-34) after 60 h under reaction conditions (30 bar, 375 °C, $H_2/CO = 3$) using ^{13}C isotope-enriched CO_2 (Fig. 5). $^{13}CO_2$ high-pressure gas is cost intensive and the experiment was carried out as a model test to measure the SAPO-34 by ^{13}C ssNMR on a dual bed configuration. Generally, one-dimensional (1D) ssNMR spectra of the post-reacted zeotype show the following three features: (i) 5–50 ppm (aliphatic), (ii) 110–150 ppm (olefinic/methylated aromatic), and (iii) 180–220 ppm (carbonyl moieties) [66–69]. We applied a series of magnetization transfer schemes based on the mobility of trapped molecules, which had been previously developed to elucidate molecular structures in zeolites [66,70,71]. For example, ^{13}C direct excitation (DE) pulse sequence has been applied to detect all chemical species in quantitative analysis, while mobile and rigid organic species can be differentiated by applying scalar-based through-bond (insensitive nuclei enhanced by polarization transfer, INEPT) and dipolar-based thorough-space (cross-polarization based, CP) magnetization transfer schemes, respectively. Such technique allowed us to distinguish between species with either weak interaction or adsorbed on the zeotype.

The 1D ^{13}C DE MAS ssNMR spectra show high amounts of aromatics-

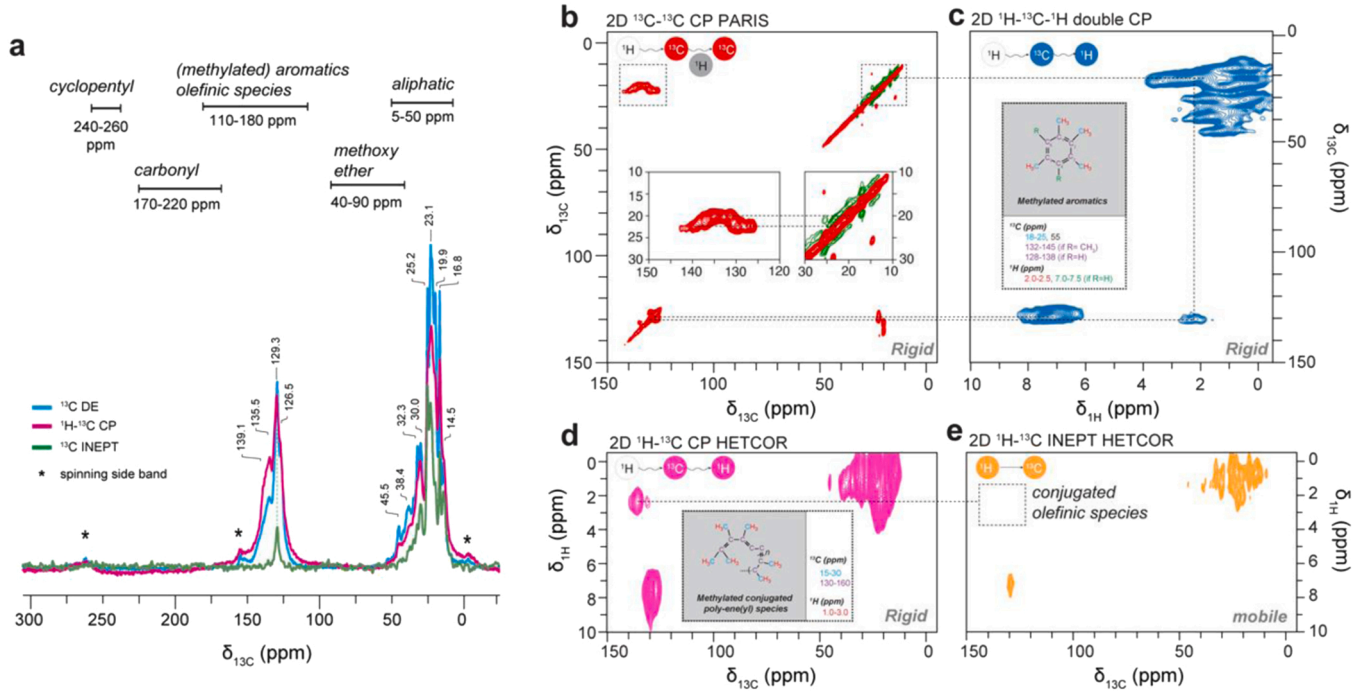

Fig. 5. (a) 1D ^{13}C DE, ^{1}H–^{13}C CP, ^{1}H–^{13}C INEPT ssNMR MAS spectra of post-reacted SAPO-34 zeotype after hydrogenation of CO_2 of fully isotope-enriched $^{13}CO_2$ in the reactant feed ($^{13}CO_2$ at 30 bar, 375 °C, $H_2/^{13}CO_2 = 3$, and 10000 ml g^{-1} h^{-1} at a time-on-stream of 60 h). 2D ssNMR correlation spectra acquired using (b) 2D ^{13}C–^{13}C, (c) 2D ^{1}H–^{13}C-^{1}H, (d) ^{1}H–^{13}C CP HETCOR, and (e) ^{1}H–^{13}C INEPT HETCOR. MAS spinning rate at 20 kHz and the spinning side bands are noted with asterisk.

related species in spent SAPO-34. Moreover, the species typically observed in the initial and steady-state stages during methanol-to-hydrocarbons, such as methoxy (13 C, 1 H = 57.7, 3.5 ppm), methanediol (93.1, 4.9 ppm), dimethoxymethane (100, 4.7 ppm), and DME (62.4, 3.46 ppm) are not observed, which again indicates that the spent sample was obtained at the deactivation stage, which is in line with the activity test results (Fig. 1). By applying ^{1}H–^{13}C CP magnetization transfer scheme, alkane species can be enhanced due to higher proton density around ^{13}C nuclei of interest (H/C ratio of alkane = ca. 1.7; aromatics = 1 (benzene), 1.25 (xylene), respectively) [70]. Most of the observed species in INEPT based pulse are confidently assigned as terminal alkyl groups from methylated aromatics or polyaromatics, i.e., most of the trapped aromatics are rigid aromatic species. This is confirmed by applying 2D ^{13}C–^{13}C and ^{1}H–^{13}C-^{1}H correlation spectra, which was achieved through proton-driven spin diffusion using phase alternated recoupling irradiations schemes (PDSD PARIS) and proton detected CP-based hetero-nuclear correlation spectroscopy (double CP-HETCOR) (Fig. 5-b, c). For example, methylated aromatic species is readily observed at 135.2/20.0 and 131.3/19.9 ($^{13}C/^{13}C$), showing their correlation with ^{1}H at 7.2 ppm [72]. According to the hydrocarbon pool mechanism [29], the C_3 families are mostly produced by two competing cycles governed by olefinic and aromatic cycles [73]. Although the sample was obtained at deactivation stage, we could see the traces of methylated olefinic species, indicating SAPO-34 has experienced dual-cycle mechanism, responsible for high C_3 selectivity. The methylated poly-ene species are previously reported as rigid compounds, showing ^{13}C and ^{1}H chemical shift ranges at 130–160 and 1–3 ppm [70], respectively. In spent SAPO-34, we could observe the cross-peaks at 136.5/2.3 and 131.4/2.4 ($^{13}C/^{1}H$) ppm by 2D ^{1}H–^{13}C CP-HETCOR but not by INEPT-HETCOR, indicating the presence of less-mobile methylated alkene species, which are presumably adsorbed in the zeotype framework (Fig. 5-d, e).

4. Conclusions

In this work, we have focused on the characterization of a combined system eligible as candidate for carbon dioxide hydrogenation into methanol and conversion to hydrocarbons. This system has shown to be highly active and selective for C_3 hydrocarbon production, in particular propane [31]. This attitude can be directly correlated to the formation of a PdZn alloy on the $PdZn/ZrO_2$ component that has been confirmed in our previous paper [31] and well demonstrated by FT-IR findings. Indeed, using CO as a probe molecule on the lone $PdZn/ZrO_2$ catalyst, the position of the IR band related to Pd^0 linear carbonyls and the absence of bridged carbonyls are ascribable to the formation of the alloy. NAP-XPS study of $PdZn/ZrO_2$ catalyst, as prepared and after reduction, confirms the formation of a PdZn alloy. Indeed, in good agreement with the literature data [45,46,48], we observe a shift of 1 eV in binding energy after reduction when comparing the $PdZn/ZrO_2$ catalyst to a model of Pd foil submitted to similar conditions. Moreover, FT-IR spectra of CO adsorbed at LNT show a particular behavior of Pd^0 carbonyl band, which we named *"bell-shaped shift"*, due to the CO adsorption onto Zn^{2+} and Zr^{4+} sites of the oxidic phases in intimate contact with the PdZn alloy particles. The presence of a residual ZnO phase after reduction is demonstrated by NAP-XPS measurements that confirm previously obtained results [31].

When the metal-oxide phase is mechanically mixed with the zeotype SAPO-34, the characteristic spectroscopic features of the two components obtained after CO adsorption at LNT do not appear perturbed by the mixing. Nevertheless, after catalytic testing, aromatic and aliphatic compounds cover Pd sites and decrease the amount of Brønsted acid sites of SAPO-34. Indeed, as confirmed by ssNMR results, high amount of aromatic and olefinic species are present, indicating that SAPO-34 underwent a dual-cycle mechanism, responsible for high C_3 selectivity. Regeneration (i.e. oxidation at 600 °C) is mandatory to restore the catalytic sites of the combined system; however, after the regeneration, a small fraction of Pd^{2+} and possibly Zn^{2+} exchanges some Brønsted acid sites inside the zeotype, which, after repeated regeneration cycles, could be one of the causes of the reduction of the catalytic activity in propane formation.

CRediT authorship contribution statement

Pierfrancesco Ticali: Investigation, Data curation, Writing – original draft, Visualization. **Sara Morandi:** Conceptualization, Writing – review & editing. **Genrikh Shterk:** Investigation, Data curation, Writing – original draft. **Samy Ould-Chikh:** Writing – review & editing. **Adrian Ramirez:** Investigation, Data curation, Writing – original draft. **Jorge Gascon:** Supervision, Funding acquisition. **Sang-Ho Chung:** Investigation, Data curation, Writing – original draft. **Javier Ruiz-Martinez:** Writing – review & editing. **Silvia Bordiga:** Supervision, Funding acquisition, Writing – review & editing.

Declaration of Competing Interest

The authors declare the following financial interests/personal relationships which may be considered as potential competing interests. Silvia Bordiga reports financial support was provided by European Union.

Data availability

Data will be made available on request.

Acknowledgements

This project has received funding from the European Union's Horizon 2020 Research and Innovation Programme under grant agreement No. 837733. The authors are grateful to Dr. Christian Ahoba-Sam for the synthesis of the $PdZn/ZrO_2$ sample.

Appendix A. Supplementary material

Supplementary data associated with this article can be found in the online version at doi:10.1016/j.apcata.2023.119100.

References

[1] NOAA ESRL Global Monitoring Laboratory, Trends in Atmospheric Carbon Dioxide, 2020. ⟨https://gml.noaa.gov/ccgg/trends/mlo.html⟩.
[2] K. Li, J.G. Chen, ACS Catal. 9 (2019) 7840–7861, https://doi.org/10.1021/acscatal.9b01943.
[3] S. Kattel, P. Liu, J.G. Chen, J. Am. Chem. Soc. 139 (2017) 9739–9754, https://doi.org/10.1021/jacs.7b05362.
[4] J.A. Rodriguez, P. Liu, D.J. Stacchiola, S.D. Senanayake, M.G. White, J.G. Chen, ACS Catal. 5 (2015) 6696–6706, https://doi.org/10.1021/acscatal.5b01755.
[5] J. Wambach, A. Baiker, A. Wokaun, Phys. Chem. Chem. Phys. 1 (1999) 5071–5080, https://doi.org/10.1039/A904923A.
[6] W. Wang, S. Wang, X. Ma, J. Gong, Chem. Soc. Rev. 40 (2011) 3703–3727, https://doi.org/10.1039/c1cs15008a.
[7] Y. Amenomiya, Appl. Catal. A Gen. 30 (1987) 57–68.
[8] T. Fujitani, I. Nakamura, Bull. Chem. Soc. Jpn 75 (2002) 1393–1398, https://doi.org/10.1246/bcsj.75.1393.
[9] J. Wang, G. Li, Z. Li, C. Tang, Z. Feng, H. An, H. Liu, T. Liu, C. Li, Sci. Adv. 3 (2017) 1–11, https://doi.org/10.1126/sciadv.1701290.
[10] S. Kattel, P.J. Ramírez, J.G. Chen, J.A. Rodriguez, P. Liu, Science 355 (2017) 1296–1299, https://doi.org/10.1126/science.aal3573.
[11] V.V. Rozanov, O.V. Krylov, Russ. Chem. Rev. 66 (1997) 107–119, https://doi.org/10.1070/RC1997v066n02ABEH000308.
[12] W.C. Conner, J.L. Falconer, Chem. Rev. 95 (1995) 759–788.
[13] J. Ye, C. Liu, D. Mei, Q. Ge, ACS Catal. 3 (2013) 1296–1306, https://doi.org/10.1021/cs400132a.
[14] G. Cerrato, S. Bordiga, S. Barbera, C. Morterra, Surf. Sci. 377–379 (1997) 50–55, https://doi.org/10.1016/S0039-6028(96)01348-9.
[15] K. Tanabe, Mater. Chem. Phys 13 (1985) 347–364, https://doi.org/10.1016/0254-0584(85)90064-1.
[16] O.A. Ojelade, S.F. Zaman, J. CO_2 Util. 47 (2021), 101506, https://doi.org/10.1016/j.jcou.2021.101506.

[17] O.A. Ojelade, S.F. Zaman, Catal. Surv. Asia 24 (2020) 11–37, https://doi.org/10.1007/s10563-019-09287-z.
[18] O.A. Ojelade, S.F. Zaman, M.A. Daous, A.A. Al-Zahrani, A.S. Malik, H. Driss, G. Shterk, J. Gascon, Appl. Catal. A Gen. 584 (2019), https://doi.org/10.1016/j.apcata.2019.117185.
[19] A.S. Malik, S.F. Zaman, A.A. Al-Zahrani, M.A. Daous, J. Ind. Eng. Chem. 103 (2021) 67–79, https://doi.org/10.1016/J.JIEC.2021.07.019.
[20] S. Fakhruz Zaman, A. Shan Malik, A. Ahmed Alzahrani, M.A. Daous, L.A. Petrov, Ceria Supported Palladium/Calcium Catalyst for Hydrogenating CO2 to Dimethyl Ether, 2020.
[21] O.A. Ojelade, S.F. Zaman, CO2 Hydrogenation to Methanol over PdZn/CeO2 Catalyst, 2019. ⟨http://www.proceedings.bas.bg/DOI/doi2019_6_05.html⟩, ⟨https://doi.org/10.7546/CRABS.2019.06.05⟩.
[22] A.S. Malik, S.F. Zaman, A.A. Al-Zahrani, M.A. Daous, H. Driss, L.A. Petrov, Catal. Today 357 (2020) 573–582, https://doi.org/10.1016/j.cattod.2019.05.040.
[23] K. Cheng, B. Gu, X. Liu, J. Kang, Q. Zhang, Y. Wang, Angew. Chem. Int. Ed. 55 (2016) 4725–4728, https://doi.org/10.1002/anie.201601208.
[24] F. Jiao, J. Li, X. Pan, J. Xiao, H. Li, H. Ma, M. Wei, Y. Pan, Z. Zhou, M. Li, S. Miao, J. Li, Y. Zhu, D. Xiao, T. He, J. Yang, F. Qi, Q. Fu, X. Bao, Science 351 (80) (2016) 1065–1068, https://doi.org/10.1126/science.aaf1835.
[25] S. Wang, P. Wang, Z. Qin, Y. Chen, M. Dong, J. Li, K. Zhang, P. Liu, J. Wang, W. Fan, ACS Catal. 8 (2018) 5485–5505, https://doi.org/10.1021/acscatal.8b01054.
[26] T. Liang, J. Chen, Z. Qin, J. Li, P. Wang, S. Wang, G. Wang, M. Dong, W. Fan, J. Wang, ACS Catal. 6 (2016) 7311–7325, https://doi.org/10.1021/acscatal.6b01771.
[27] R.M. Dessau, R.B. LaPierre, J. Catal. 78 (1982) 136–141, https://doi.org/10.1016/0021-9517(82)90292-5.
[28] I.M. Dahl, S. Kolboe, Catal. Lett. 20 (1993) 329–336, https://doi.org/10.1007/BF00769305.
[29] W. Wang, Y. Jiang, M. Hunger, Catal. Today 113 (2006) 102–114, https://doi.org/10.1016/J.CATTOD.2005.11.015.
[30] PRopane Market – Growth, Trends, and Forecast (2020–2025), n.d.
[31] A. Ramirez, P. Ticali, D. Salusso, T. Cordero-Lanzac, S. Ould-Chikh, C. Ahoba-Sam, A.L. Bugaev, E. Borfecchia, S. Morandi, M. Signorile, S. Bordiga, J. Gascon, U. Olsbye, JACS Au 1 (2021) 1719–1732, https://doi.org/10.1021/jacsau.1c00302.
[32] S. De, A. Dokania, A. Ramirez, J. Gascon, ACS Catal. 10 (2020) 14147–14185, https://doi.org/10.1021/acscatal.0c04273.
[33] K.I. Hadjiivanov, G.N. Vayssilov, Adv. Catal. 47 (2002) 307–511, https://doi.org/10.1016/S0360-0564(02)47008-3.
[34] K. Föttinger, Catal. Today 208 (2013) 106–112, https://doi.org/10.1016/j.cattod.2012.12.004.
[35] T. Conant, A.M. Karim, V. Lebarbier, Y. Wang, F. Girgsdies, R. Schlögl, A. Datye, J. Catal. 257 (2008) 64–70, https://doi.org/10.1016/j.jcat.2008.04.018.
[36] C. Rameshan, W. Stadlmayr, C. Weilach, S. Penner, H. Lorenz, M. Hävecker, R. Blume, T. Rocha, D. Teschner, A. Knop-Gericke, R. Schlögl, N. Memmel, D. Zemlyanov, G. Rupprechter, B. Klötzer, Angew, Chem. Int. Ed. 49 (2010) 3224–3227, https://doi.org/10.1002/anie.200905815.
[37] P. Hollins, Surf. Sci. Rep. 16 (1992) 51–94, https://doi.org/10.1016/0167-5729(92)90008-Y.
[38] P. Hollins, J. Pritchard, Surf. Sci. 89 (1979) 486–495, https://doi.org/10.1016/0039-6028(79)90633-2.
[39] D. Scarano, S. Bertarione, G. Spoto, A. Zecchina, C. Otero Areán, Thin Solid Films 400 (2001) 50–55, https://doi.org/10.1016/S0040-6090(01)01472-9.
[40] C. Morterra, V. Bolis, B. Fubini, L. Orio, T.B. Williams, Surf. Sci. 251–252 (1991) 540–545, https://doi.org/10.1016/0039-6028(91)91051-X.
[41] P. Ticali, D. Salusso, R. Ahmad, C. Ahoba-Sam, A. Ramirez, G. Shterk, K. A. Lomachenko, E. Borfecchia, S. Morandi, L. Cavallo, J. Gascon, S. Bordiga, U. Olsbye, Catal. Sci. Technol. 11 (2021) 1249–1268, https://doi.org/10.1039/D0CY01550D.
[42] A.I. Serykh, Y.A. Agafonov, Mol. Catal. 493 (2020), 111055, https://doi.org/10.1016/j.mcat.2020.111055.
[43] R.M. Hammaker, S.A. Francis, R.P. Eischens, Spectrochim. Acta 21 (1965) 1295–1309.
[44] B.N.J. Persson, R. Ryberg, Phys. Rev. B 24 (1981) 6954–6970, https://doi.org/10.1103/PhysRevB.24.6954.
[45] A. Bayer, K. Flechtner, R. Denecke, H.-P. Steinrück, K.M. Neyman, N. Rösch, Surf. Sci. 600 (2006) 78–94, https://doi.org/10.1016/j.susc.2005.09.049.
[46] H.H. Holzapfel, A. Wolfbeisser, C. Rameshan, C. Weilach, G. Rupprechter, Top. Catal. 57 (2014) 1218–1228, https://doi.org/10.1007/s11244-014-0295-3.
[47] C. Rameshan, C. Weilach, W. Stadlmayr, S. Penner, H. Lorenz, M. Hävecker, R. Blume, T. Rocha, D. Rocha, A. Knop-Gericke, J. Catal. 276 (2010) 101–113, https://doi.org/10.1016/j.jcat.2010.09.006.
[48] C. Rameshan, W. Stadlmayr, C. Weilach, S. Penner, H. Lorenz, M. Hävecker, R. Blume, T. Rocha, D. Teschner, A. Knop-Gericke, R. Schlögl, N. Memmel, D. Zemlyanov, G. Rupprechter, B. Klötzer, Angew. Chem. Int. Ed. 49 (2010) 3224–3227, https://doi.org/10.1002/anie.200905815.
[49] N. Iwasa, S. Masuda, N. Ogawa, N. Takezawa, Appl. Catal. A Gen. 125 (1995) 145–157, https://doi.org/10.1016/0926-860X(95)00004-6.
[50] J.A. Rodriguez, J. Phys. Chem. 98 (1994) 5758–5764, https://doi.org/10.1021/j100073a031.
[51] K.M. Neyman, R. Sahnoun, C. Inntam, S. Hengrasmee, N. Rösch, J. Phys. Chem. B 108 (2004) 5424–5430, https://doi.org/10.1021/jp049830f.
[52] Z.-X. Chen, K.M. Neyman, A.B. Gordienko, N. Rösch, Phys. Rev. B 68 (2003), 075417, https://doi.org/10.1103/PhysRevB.68.075417.
[53] K.M. Neyman, K.H. Lim, Z.-X. Chen, L.V. Moskaleva, A. Bayer, A. Reindl, D. Borgmann, R. Denecke, H.-P. Steinrück, N. Rösch, Phys. Chem. Chem. Phys. 9 (2007) 3470–3482, https://doi.org/10.1039/B700548B.
[54] M. Friedrich, A. Ormeci, Y. Grin, M. Armbrüster, Z. Anorg. Allg. Chem. 636 (2010) 1735–1739, https://doi.org/10.1002/zaac.201000097.
[55] A.V. Naumkin, A. Kraut-Vass, S.W. Gaarenstroom, C.J. Powell, NIST Standard Reference Database 20, Version 4.1 (Web Version), 2012.
[56] M.C. Militello, S.J. Simko, Surf. Sci. Spectra 3 (1994) 395–401, https://doi.org/10.1116/1.1247784.
[57] M. Brun, A. Berthet, J. Bertolini, J. Electron Spectrosc. Relat. Phenom. 104 (1999) 55–60, https://doi.org/10.1016/S0368-2048(98)00312-0.
[58] C. Huang, Z. Wu, H. Luo, S. Zhang, Z. Shao, H. Wang, Y. Sun, ACS Appl. Energy Mater. 4 (2021) 9258–9266, https://doi.org/10.1021/acsaem.1c01502.
[59] F. Bleken, M. Bjørgen, L. Palumbo, S. Bordiga, S. Svelle, K.P. Lillerud, U. Olsbye, Top. Catal. 52 (2009) 218–228, https://doi.org/10.1007/s11244-008-9158-0.
[60] V. Bolis, B. Fubini, E. Garrone, E. Giamello, C. Morterra, Stud. Surf. Sci. Catal. 48 (1989) 159–166, https://doi.org/10.1016/S0167-2991(08)60679-5.
[61] S. Bordiga, E. Escalona Platero, C. Otero Areán, C. Lamberti, A. Zecchina, J. Catal. 137 (1992) 179–185, https://doi.org/10.1016/0021-9517(92)90147-A.
[62] S. Bordiga, D. Scarano, G. Spoto, A. Zecchina, C. Lamberti, C. Otero Areán, Vib. Spectrosc. 5 (1993) 69–74, https://doi.org/10.1016/0924-2031(93)87056-Y.
[63] C. Ahoba-Sam, E. Borfecchia, A. Lazzarini, A. Bugaev, A.A. Isah, M. Taoufik, S. Bordiga, U. Olsbye, Catal. Sci. Technol. (2020) 4373–4385, https://doi.org/10.1039/D0CY00440E.
[64] K. Khivantsev, N.R. Jaegers, L. Kovarik, J.C. Hanson, F. (Feng) Tao, Y. Tang, X. Zhang, I.Z. Koleva, H.A. Aleksandrov, G.N. Vayssilov, Y. Wang, F. Gao, J. Szanyi, Angew. Chem. Int. Ed. 57 (2018) 16672–16677, https://doi.org/10.1002/anie.201809343.
[65] L. Castoldi, R. Matarrese, S. Morandi, P. Ticali, L. Lietti, Catal. Today 360 (2021) 317–325, https://doi.org/10.1016/j.cattod.2020.02.019.
[66] A. Ramirez, X. Gong, M. Caglayan, S.-A.F. Nastase, E. Abou-Hamad, L. Gevers, L. Cavallo, A. Dutta Chowdhury, J. Gascon, Nat. Commun. 12 (2021) 5914, https://doi.org/10.1038/s41467-021-26090-5.
[67] M. Çağlayan, A. Lucini Paioni, E. Abou-Hamad, G. Shterk, A. Pustovarenko, M. Baldus, A.D. Chowdhury, J. Gascon, Angew. Chem. Int. Ed. 59 (2020) 16741–16746, https://doi.org/10.1002/anie.202007283.
[68] D. Fu, A. Lucini Paioni, C. Lian, O. Heijden, M. Baldus, B.M. Weckhuysen, Angew. Chem. Int. Ed. 59 (2020) 20024–20030, https://doi.org/10.1002/anie.202009139.
[69] C. Wang, Y. Chu, J. Xu, Q. Wang, G. Qi, P. Gao, X. Zhou, F. Deng, Angew. Chem. 130 (2018) 10354–10358, https://doi.org/10.1002/ange.201805609.
[70] A.D. Chowdhury, A.L. Paioni, K. Houben, G.T. Whiting, M. Baldus, B. M. Weckhuysen, Angew. Chem. Int. Ed. 57 (2018) 8095–8099, https://doi.org/10.1002/anie.201803279.
[71] A.D. Chowdhury, K. Houben, G.T. Whiting, S.-H. Chung, M. Baldus, B. M. Weckhuysen, Nat. Catal. 1 (2017) 23–31, https://doi.org/10.1038/s41929-017-0002-4.
[72] A.D. Chowdhury, K. Houben, G.T. Whiting, M. Mokhtar, A.M. Asiri, S.A. Al-Thabaiti, S.N. Basahel, M. Baldus, B.M. Weckhuysen, Angew. Chem. 128 (2016) 16072–16077, https://doi.org/10.1002/ange.201608643.
[73] I. Yarulina, A.D. Chowdhury, F. Meirer, B.M. Weckhuysen, J. Gascon, Nat. Catal. 1 (2018) 398–411, https://doi.org/10.1038/s41929-018-0078-5.